



## **Hybrid Brazing-Adhesive Bonding of Al/Ti Dissimilar Joints Enabled by Resistance Spot Welding**

Microstructure evolution and bonding mechanisms are characterized, and the mechanical performance of joints produced by several methods is evaluated

BY M. HAMRAH AND M. POURANVARI

#### **Abstract**

Joining dissimilar materials, such as aluminum and titanium, through fusion-based techniques presents difficulties because of their considerable differences in physical properties and metallurgical incompatibility. This research employed a hybrid bonding method for joining aluminum and titanium by integrating adhesive bonding with metallurgical joining at the solid titanium and liquid aluminum interface, utilizing resistance spot welding. The experimental findings indicated that this hybrid bonding method greatly enhances the load-bearing capacity and energy absorption performance of AA6061/Ti-6Al-4V joints compared to conventional resistance spot welding.

#### **Keywords**

- Al/Ti Dissimilar Metal Joining
- Hybrid Bonding
- Resistance Spot Welding
- Solid-Liquid Interface Joining
- Microstructure
- Mechanical Properties

#### Introduction

The concept of multi-material design in manufacturing is a pivotal strategy that focuses on choosing the most suitable materials for each part of an assembly according to specific service demands. This approach is fundamentally linked to the practice of dissimilar metal welding (Ref. 1). However, the weldability of dissimilar metals is significantly affected by discrepancies in their physical properties, including melting points, coefficients of thermal expansion, thermal conductivity, and electrical resistivity, along with potential metallurgical incompatibilities (Refs. 1-7).

The joining of aluminum and titanium (Al/Ti), which is essential for lightweight design concepts in various transportation systems, faces challenges due to two key factors:

- 1. There are significant differences in their physical properties. These differences include melting points (660°C for Al vs. 1668°C for Ti), electrical resistivity (0.028  $\mu\Omega$ .m for Al and 0.42–0.52  $\mu\Omega$ .m for Ti), thermal conductivity (234 W/ mK for Al vs. 16 W/mK for Ti), thermal expansion coefficient  $(23.6 \times 10^{-6})$  1/K for Al vs.  $8.6 \times 10^{-6}$  1/K for Ti) (Ref. 8); and
- 2. Metallurgical incompatibility (i.e., very limited solid solubility), resulting in the formation of intermetallic compounds (e.g., TiAl and TiAl<sub>2</sub>) at the joint interface (Refs. 9–13).

Joining aluminum and titanium through dissimilar metallurgical methods can be accomplished via three types of interfaces: solid/solid interface (such as friction stir welding [Ref. 6]), solid/liquid interface (like laser brazing [Refs. 10, 11] and resistance spot welding [Refs. 12, 13]), and liquid/ liquid interface (i.e., fusion welding [Ref. 9]). However, the formation of intermetallic compounds often weakens the joints produced by these techniques (Refs. 9-13). To mitigate this issue, adhesive bonding can be a joining method complementary to metallurgical bonding. Additionally, adhesive bonding offers two key advantages in lap joint applications: uniform load distribution and reduced stress concentration (Refs. 14-16). Despite these benefits, adhesive bonds generally exhibit lower resistance than welded joints to normal and peeling forces (Ref. 17). A hybrid joining approach, combining metallurgical and adhesive bonding, can leverage the strengths of both methods.

Recently, hybrid techniques for joining dissimilar metals have gained considerable attention. For example, Liu et al. (Ref. 18) reported that laser weld-bonding of Al/Mg dissimilar joints, which integrates laser fusion welding with adhesive bonding, increased joint strength by over 30 times compared

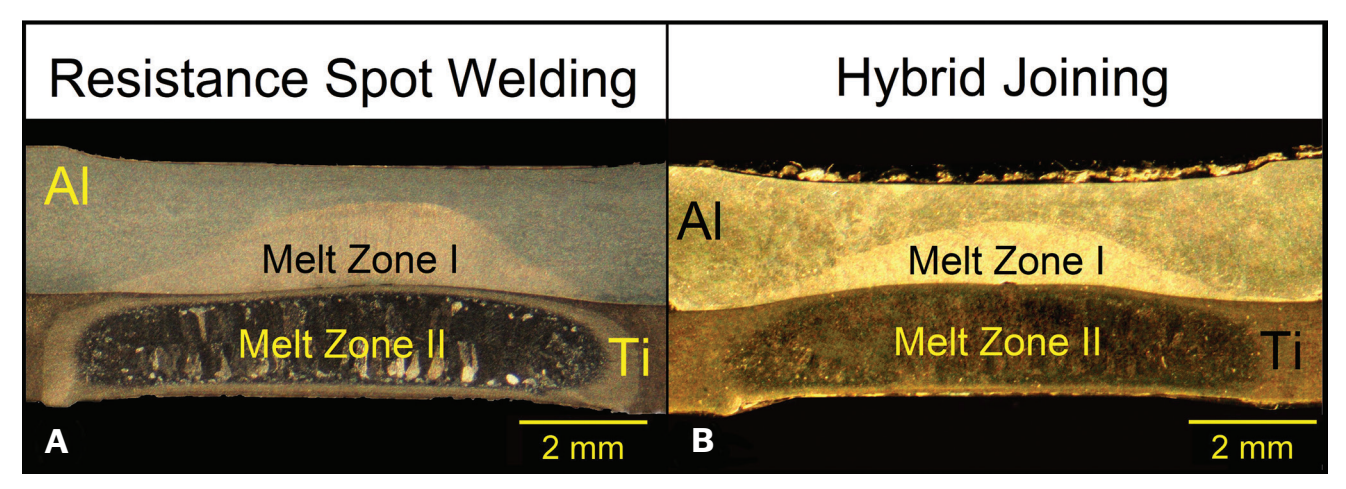


Fig. 1 — Macrostructure of Al/Ti joints made using: A — Resistance spot welding; B — hybrid joining combining resistance spot welding and adhesive bonding.

to brittle, low-strength laser-welded joints plagued by coarse intermetallic compounds. Miyamoto et al. (Ref. 19) demonstrated that combining adhesive bonding with resistance spot welding for Al/steel joints improves corrosion resistance due to the sealing effect of the adhesive. Kang et al. (Ref. 20) found that adding adhesive bonding to resistance spot welding increased porosity in the melt zone. While the melted zone size expanded, the tensile-shear peak load remained similar to conventional spot welding. Chen et al. (Ref. 21) achieved a 2.3-fold increase in tensile-shear strength for Al/steel joints by implementing a two-step weld-bonding process (pre-cleaning followed by welding) and using a multistep face electrode. Furthermore, resistance element welding (REW) and resistance rivet welding (RRW) are cost-intensive mechanical-metallurgical hybrid techniques developed for joining dissimilar metals, such as Al and Ti (Refs. 22, 23). In REW, a titanium rivet is inserted into a pre-drilled hole in the Al sheet then resistance-welded to the Ti sheet, effectively transforming the joint interface into a similar material region (Ref. 22). In contrast, RRW eliminates the need for pre-drilling and instead forms a localized molten nugget composed of mixed Al and Ti, which helps reduce the formation of brittle intermetallic compounds at the interface (Ref. 23).

Given the limitations of resistance spot welding (RSW) in producing high-strength Al/Ti dissimilar joints (Ref. 12), this study explored a hybrid joining strategy that integrated adhesive bonding (AB) with RSW. In this approach, RSW supplied the required thermal input. At the same time, joint formation primarily occurred via a solid-liquid reaction (i.e., a brazing mechanism) at the Al/Ti interface, synergistically complemented by adhesive bonding, hereafter termed hybrid brazing-adhesive bonding (HB). The microstructure evolution and bonding mechanisms were characterized, and the mechanical performance of joints produced by RSW, AB, and HB was evaluated.

### **Materials and Methods**

This work utilized AA6061-T6 aluminum sheets with a thickness of 2 mm and Ti6Al4V titanium sheets measuring 1.5 mm

in thickness as the base materials. The chemical composition of the AA6061-T6 aluminum alloy was AI-1.12Mg-0.605Si-0.357Fe-0.263Cu (in wt-%), while the Ti6Al4V alloy comprised Ti-6.4AI-4.2V-0.05Fe-0.02Cu (in wt-%). The AA6061-T6 alloy exhibited a tensile strength of 282 MPa and a total elongation of 17%, whereas the Ti6Al4V alloy demonstrated a tensile strength of 1090 MPa with an elongation of 10%.

Rectangular specimens with dimensions of 100 mm × 25 mm were fabricated for joint fabrication experiments in accordance with AWS D17.2, *Specification for Resistance Welding for Aerospace Applications* (Ref. 24). A three-stage cleaning process was implemented to ensure consistent surface cleanliness and optimal bonding conditions. This approach involved the initial degreasing of the specimen surfaces using acetone to eliminate contaminants. Subsequently, scratch brushing was performed to remove oxide layers, followed by a final degreasing step using acetone.

We employed three distinct methods for joining the dissimilar materials AA6061 and Ti6Al4V: resistance spot welding, adhesive bonding, and hybrid-bonding. Each method was carried out as follows:

1. Resistance spot welding: The RSW process was executed using a PLC-controlled, 100 kVA AC pedestal RSW machine. A 45-deg truncated cone electrode, classified as RWMA Class 2, with an 8-mm face diameter, was employed for the operation. The welding parameters included a squeeze time of 0.5 s, a welding time of 0.17 s, a welding current of 13 kA, a post-current electrode holding time of 0.17 s, and an electrode force of 5 kN.

2. Adhesive bonding: For the adhesive bonding process, we utilized Bylapox 3125 HV, a solvent-free two-component epoxy resin adhesive enhanced with rubber for improved performance. Prior to application, the epoxy resin and hardener were combined in equal proportions (1:1 ratio). The adhesive was carefully applied to the overlapping area of the sheets, measuring  $25 \times 25$  mm. To promote optimal bonding, pressure equivalent to that used in resistance spot welding was exerted. The specimens were then placed in a low-temperature furnace under controlled curing conditions, where they were heated to  $200^{\circ}\text{C}$  for 15 min, followed by a gradual cooling period.

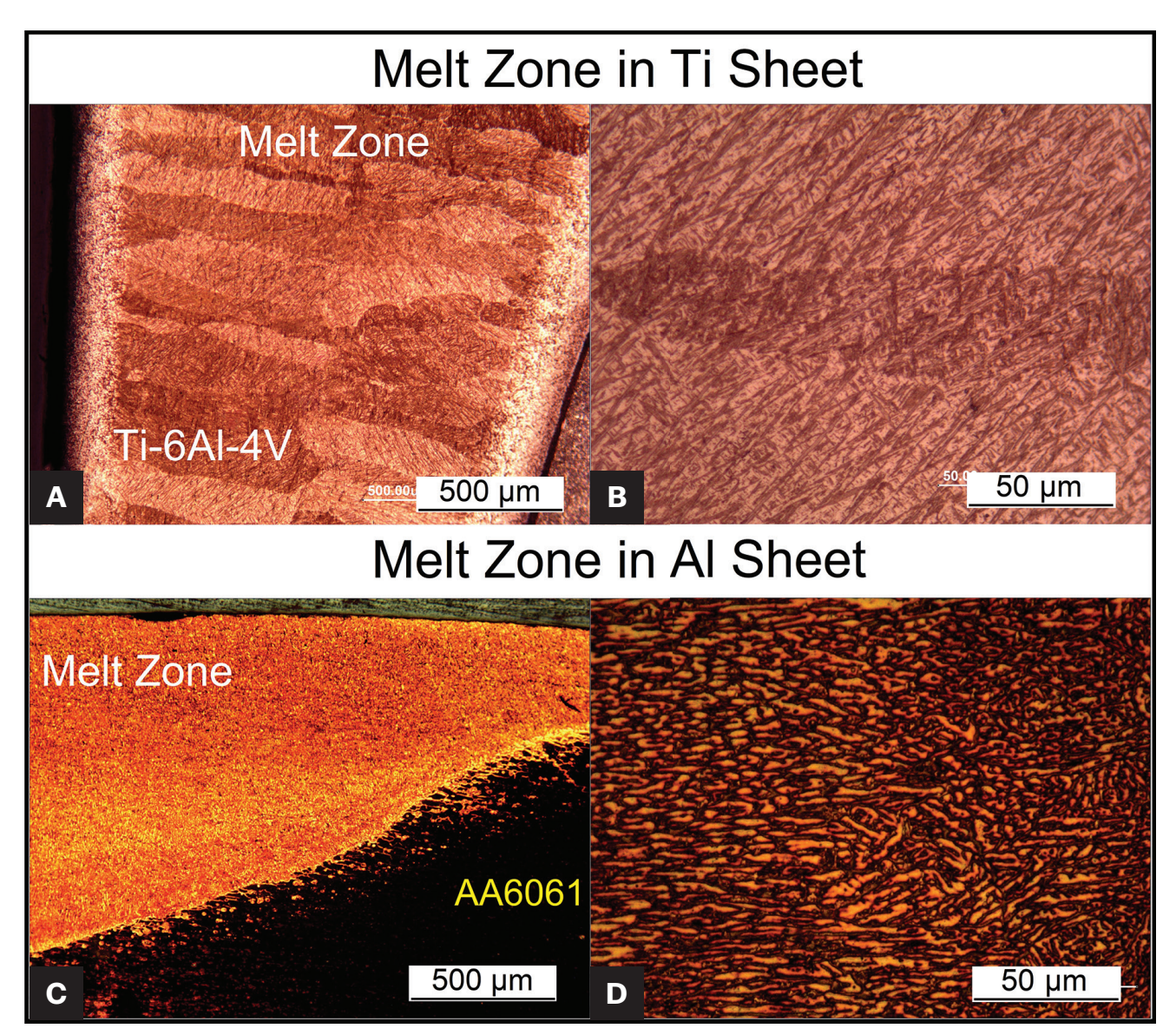


Fig. 2 — Microstructure of dissimilar Al6061/Ti-6Al-4V resistance spot welds: A–B — Melt zone in Ti-6Al-4V sheet showing the columnar grain formation (Fig. 2A) and martensitic microstructure within the grains (Fig. 2B). A dark band is visible along the interface due to differential etching response between the base metals and the interfacial region. This feature is not a crack or unbonded zone; the interface remained metallurgically continuous, as confirmed by the higher magnification micrograph shown in Fig. 3A. C-D — melt zone in AA6061 sheet showing its dendritic microstructure.

3. Hybrid-bonding: In this process, adhesive was first spread over the surfaces of the sheets, followed by resistance spot welding executed with identical parameters to those utilized in the RSW method. During the squeeze time, the electrode force displaced the adhesive layer at the joint interface, enabling direct metallic contact between the substrates. This established a conductive pathway for the electric current required for resistance welding, while the remaining adhesive layer continued to enhance joint integrity through adhesive bonding. Ultimately, the assembled joint was subjected to curing at a temperature of 200°C for a duration of 15 min.

The mechanical properties of joints produced by resistance spot welding, adhesive bonding, and hybrid-bonding were

assessed through tensile-shear testing in accordance with AWS D17.2. The tests were conducted at a crosshead speed of 2 mm/min. Load-displacement curves were recorded, and key parameters, such as peak load and failure energy (calculated as the area under the load-displacement curve up to the peak point), were extracted. The reported mechanical property values represented the average of two independent measurements. Additionally, the failure modes of the spot welds were analyzed by examining the fracture surfaces.

The metallurgical characteristics of both resistance spotwelded and hybrid-bonded joints were analyzed using light optical microscopy. Metallographic specimens were prepared in accordance with standard procedures. For macrostructural analysis, the samples were etched with a solution consisting

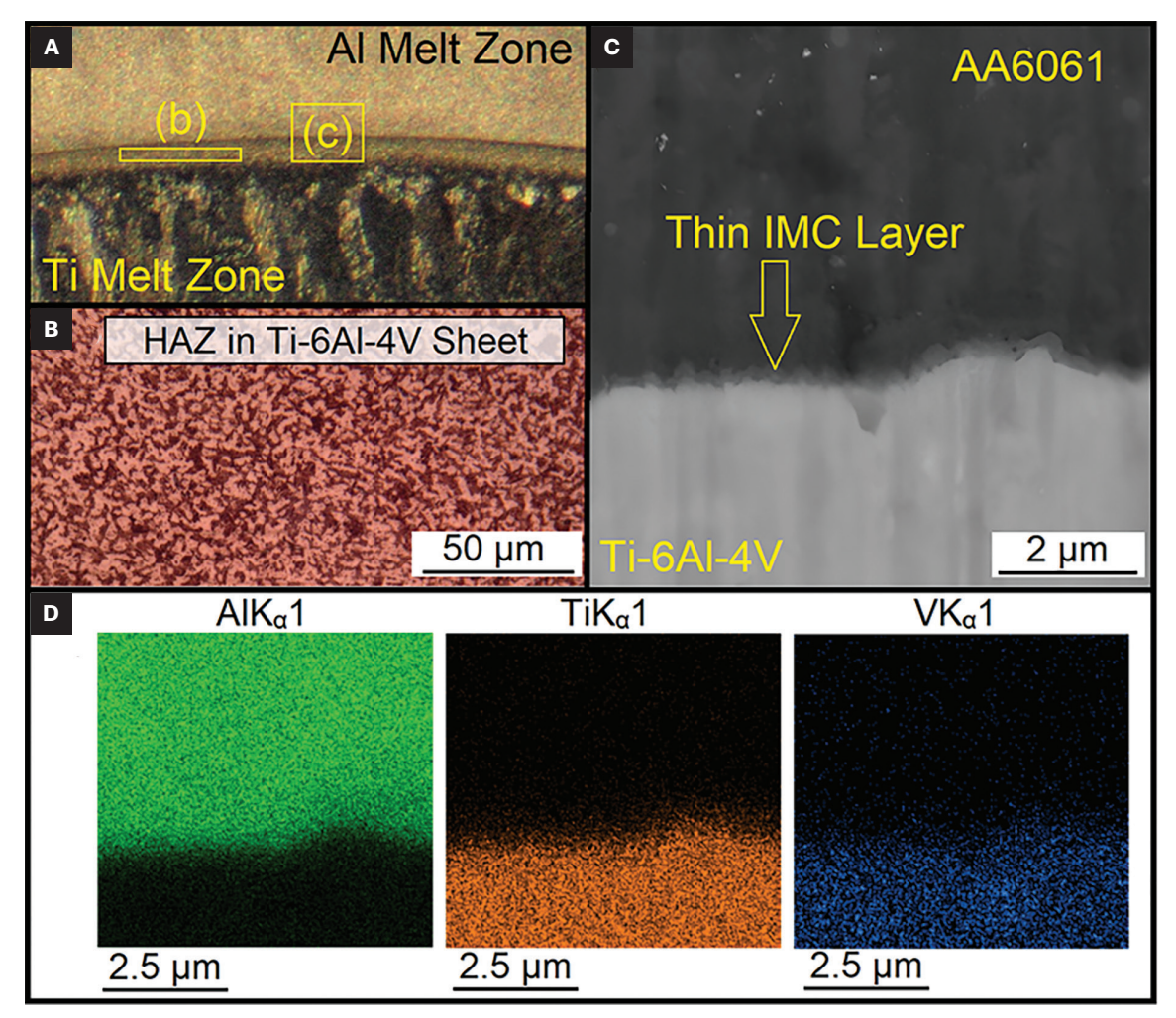


Fig. 3 — Al/Ti joint Interface: A — LOM micrograph demonstrating continuous bonding between Al and Ti; B — LOM micrograph illustrating the microstructure of the heat-affected zone (HAZ) on the Ti side near the joint interface; C — high-magnification SEM backscattered electron (BSE) image revealing the formation of an ultra-thin intermetallic compound (IMC) layer at the joint interface; D — x-ray elemental map of the joint interface.

of 2 g NH $_4$ HF $_2$ , 25 mL ethanol, and 100 mL distilled water. For microstructural analysis, the AA6061 and Ti-6Al-4V sides were etched separately using distinct solutions. The AA6061 side was etched with a solution containing 4 g KMnO $_4$ , 1 g NaOH, and 100 mL distilled water. In contrast, the Ti-6Al-4V side was etched with the same solution used for macro-examinations, which was composed of 2 g NH $_4$ HF $_2$ , 25 mL ethanol, and 100 mL distilled water.

## Results

#### Microstructure

Figure 1A shows the macrostructure of the dissimilar Al/Ti resistance spot-welded joint, while Fig. 1B presents the macrostructure of the Al/Ti hybrid-bonded joint. In both cases, metallographic analysis confirmed the presence of two distinct melt zones: melt zone I, located in the aluminum alloy, and melt zone II, within the titanium alloy. Notably, the

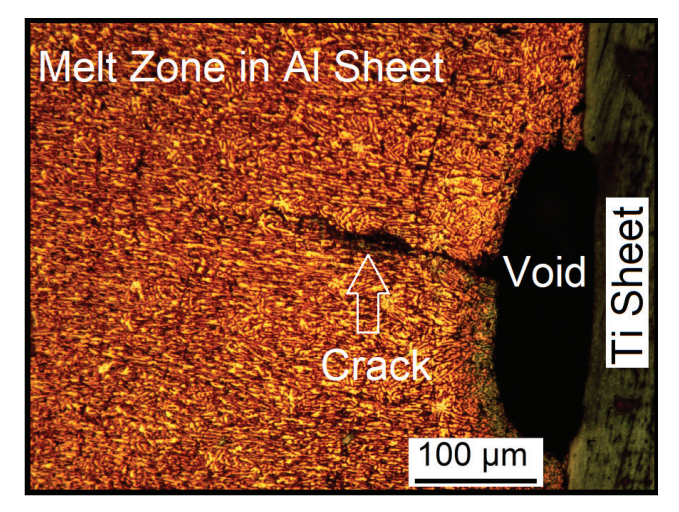


Fig. 4 — Void and crack formation at the joint interface of Al/Ti resistance spot weld.

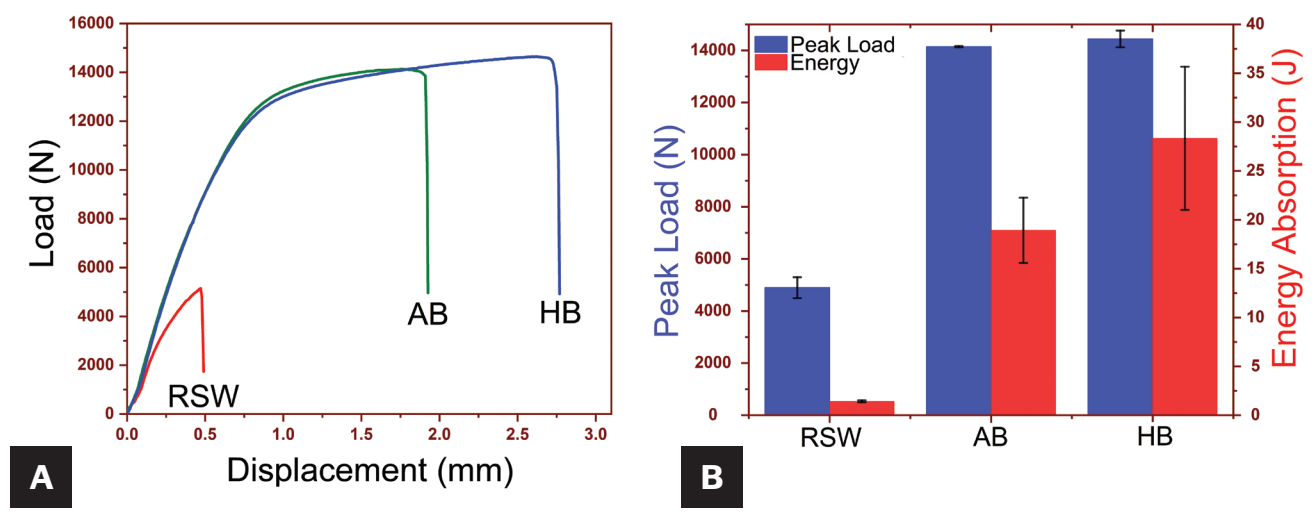


Fig. 5 — Mechanical properties of Al/Ti joint: A — Load-displacement curves; B — peak load and energy absorption of the joint made using resistance spot welding (RSW), adhesive bonding (AB), and hybrid-bonding (HB).

lengths of the solid/liquid interface, which influenced the load-bearing capacity of the joints, were 7.4 mm for the Al/ Ti RSW joint and 7.5 mm for the HB joint.

Figure 2A shows the microstructure of the melt zone within the titanium alloy in the Al/Ti RSW joint, where the presence of large columnar grains in the center of the titanium sheet confirmed that melting occurred during welding. The formation of large columnar grains was influenced by the large thermal gradient during the solidification of the melt zone. Figure 2B presents the same region, revealing the development of a martensitic structure in the titanium melt zone, which was attributed to the rapid cooling rate associated with RSW. In the aluminum sheet, Fig. 2C displays a cap-shaped melt zone formed in the AA6061 alloy, while Fig. 2D shows the dendritic microstructure within this melt zone, confirming the processes of melting and re-solidification.

It is important to note that the dark contrast observed along the joint interface in Fig. 2A is an etching-induced artifact and not indicative of any physical discontinuity or defect. This band resulted from differential etching behavior between the Al, Ti, and the interfacial region. As shown in the higher-magnification micrograph in Fig. 3A, the interface remained almost continuous and free of cracks or unbonded regions, confirming the integrity of the joint.

It is noteworthy that, as shown in Fig. 2A, the melt zone on the Ti side— characterized by a columnar grain structure — did not extend to the joint interface. A narrow band existed between the Ti melt zone and the interface, which did not undergo melting and resolidification during welding. Figure 3A presents a light optical micrograph of the Al/Ti joint interface, providing a more-detailed view of this region. The titanium adjacent to the interface exhibits a distinct etching contrast relative to the melt zone, indicating that it remained in the solid state throughout the joining process. This confirms that the Ti/Al interface formed between solid titanium and molten aluminum. Figure 3B offers a higher-magnification image of the narrow band separating the Ti melt zone from the joint interface. This region displayed microstructural features typical of a heat-affected zone (HAZ): thermally

altered but not melted. Consequently, a liquid/solid interface was established at the Al/Ti boundary, where molten aluminum met solid titanium.

Figure 3C displays a high-magnification backscattered electron SEM image of the joint interface, revealing a continuous, ultra-thin reaction layer with an average thickness of approximately 200 nm. Figure 3D provides an x-ray elemental map of the same region, highlighting a narrow transition zone between AA6061 and Ti-6Al-4V. Based on the morphology and contrast, this layer was likely an intermetallic compound (IMC) formed through an in-situ reaction between molten aluminum and solid titanium. However, further characterization using high-resolution techniques, such as transmission electron microscopy (TEM), would be necessary to confirm the exact phase composition and crystallography of this interfacial laver.

It should be noted that while a crack-free bond was formed at the Al/Ti interface, some voids were formed at the joint interface. Figure 4 shows the Al/Ti RSW joint interface, indicating the presence of a void at the joint interface. Additionally, microcracks were found near these voids.

## **Mechanical Properties**

Figure 5A shows the typical load-displacement behavior of dissimilar Al/Ti joints. Figure 5B compares the peak load and energy absorption capabilities of these different joint types. The results clearly demonstrated that resistance spot-welded joints exhibited the weakest mechanical performance, showing both the lowest peak load and minimal energy absorption capacity among all joint types examined.

HB and AB joints exhibited peak loads of 14.44  $\pm$  0.28 kN and 14.15 ± 0.02 kN, respectively. However, this difference was not statistically significant (p = 0.19), indicating that the peak load values of HB and AB joints were statistically similar.

The energy absorption values for the hybrid-bonded and adhesively bonded joints were measured to be 27.18  $\pm$  5.26 J and 17.65  $\pm$  1.49 J, respectively. Although the HB joints exhib-

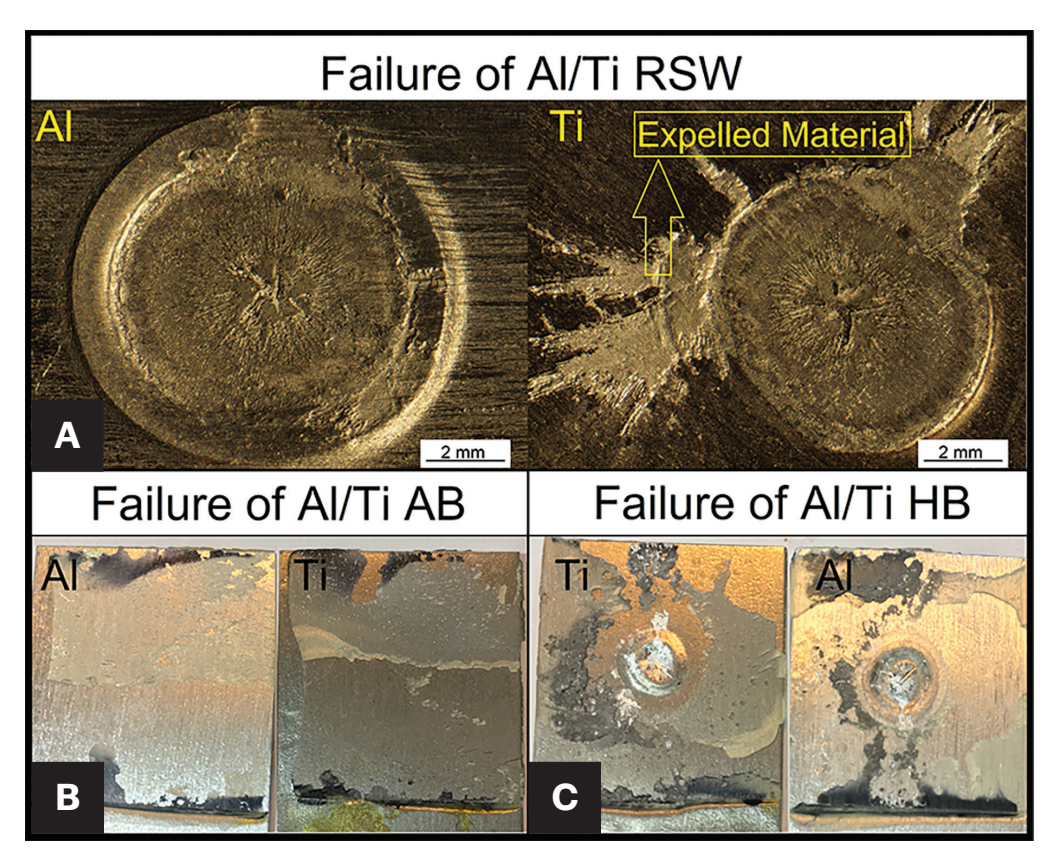


Fig. 6 — Failure of Al/Ti joints: A — Resistance spot welds; B — adhesive bonds; C — hybrid bonds.

ited a higher mean energy absorption, the difference was not statistically significant (p = 0.13), primarily due to the small sample size and high variability within the HB group. As a result, it must be concluded that the energy absorption capacities of the HB and AB joints were statistically indistinguishable based on the current dataset. To evaluate the practical significance of the observed difference, Cohen's d effect size was calculated. Cohen's d is a standardized metric that quantifies the magnitude of the difference between two means, independent of sample size (Ref. 25). Conventionally, a Cohen's d of 0.2 is considered a small effect, 0.5 medium, and 0.8 or greater a large effect (Ref. 26). This study obtained a Cohen's d of 2.3, indicating a large effect size. This suggests that the observed difference in energy absorption may be practically meaningful despite the lack of statistical significance. Notably, both HB samples consistently exhibited higher energy absorption than their AB counterparts. It is important to differentiate between statistical significance (as measured by p-value) and practical significance (as measured by effect size). While a p-value assesses the probability that an observed difference could arise by chance, Cohen's d provides insight into the strength of that difference regardless of sample size. In this context, the large effect size strongly favors the HB joints in terms of energy absorption performance. Nonetheless, further testing with a larger number of replicates is necessary to validate the reliability and reproducibility of this trend.

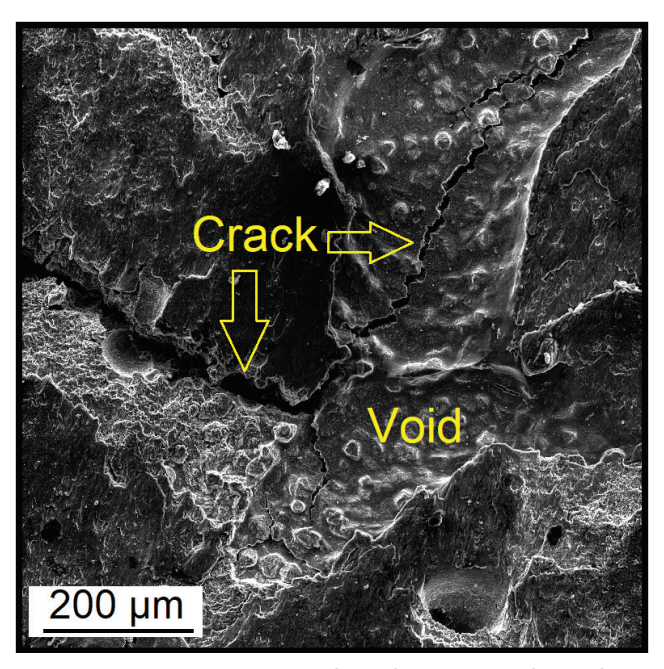


Fig. 7 — SEM micrograph of the fracture surface of Al/Ti resistance spot welds which failed along the joint interface during the tensile-shear loading. The presence of void and crack is evident on the fracture surface.

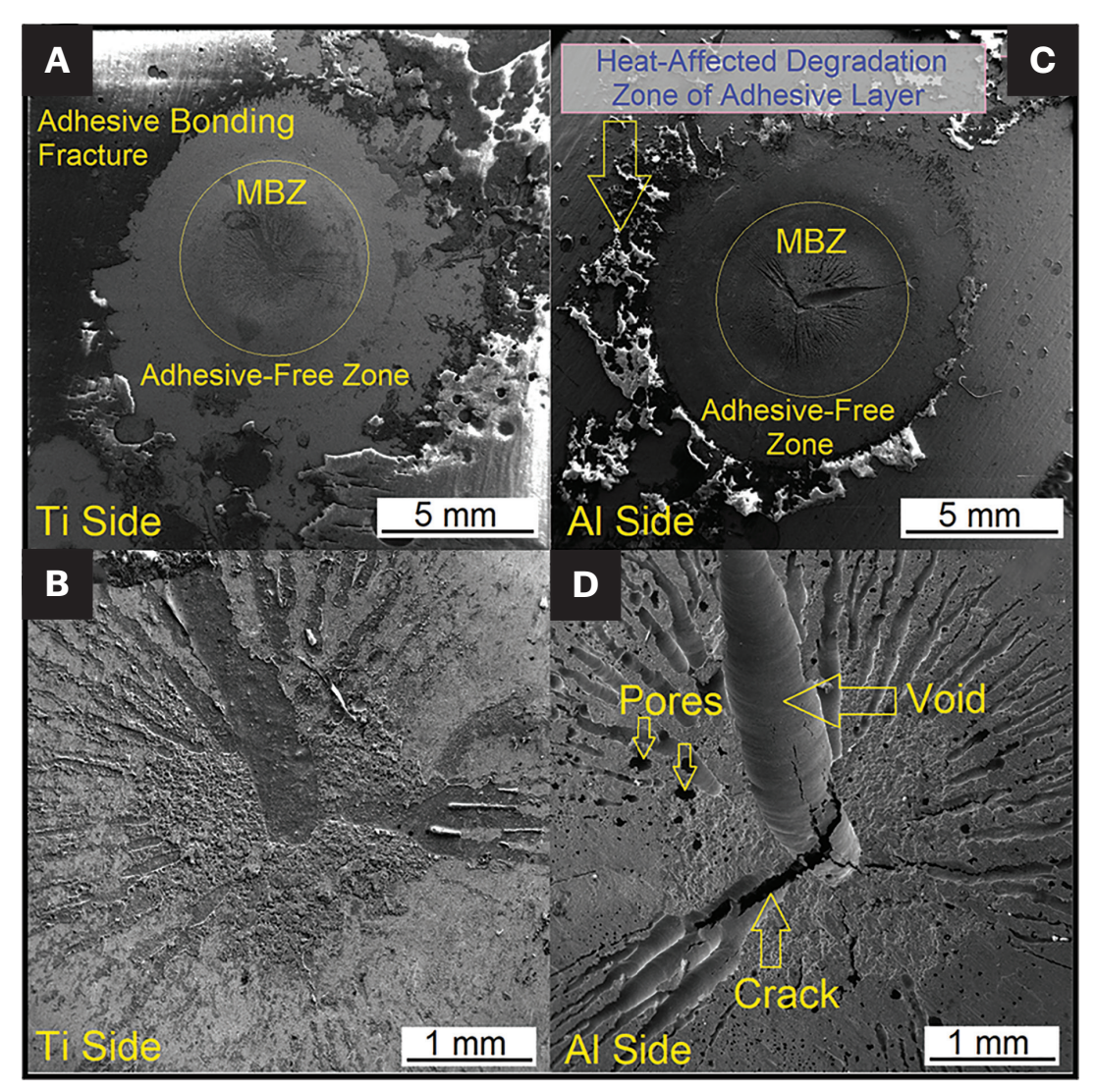


Fig. 8 — SEM analysis of the fracture surface in the Al/Ti hybrid-bonded (HB) joint: A — Overview of the Ti side; B- detailed view of the metallurgical bonding zone (MBZ) on the Ti side; C- overview of the Al side; Ddetailed view of the MBZ on the Al side. The fracture surface reveals four distinct regions, including fracture within the metallurgical bonding zone (MBZ), adhesive-free zone, and heat-affected adhesive-degraded zone, and failure of the adhesive-bonded zone. Pores, voids, and cracks are evident on the fracture surface.

#### **Failure Modes**

Understanding failure modes is crucial for assessing the integrity of joints. This section delves into the various failure modes identified in resistance spot-welded, adhesive bonded, and hybrid-bonded joints as observed during tensile-shear testing:

■ Failure Mode of RSW Joints: Resistance spot-welded joints typically exhibit two main types of failure: interfacial failure and pullout failure (Ref. 27). Interfacial failure occurs when the fracture occurs along the boundary between the two sheets. In contrast, pullout failure happens when the weld nugget separates from one of the sheets under load. Figure 6A demonstrates the interfacial failure mode in the Al/Ti RSW joint. Voids are visible at the fracture surface (i.e., joint interface). Additionally, expelled material is visible on the fracture surface, as illustrated in Fig. 6A. Figure 7 shows

the SEM fractography, indicating the presence of voids and cracks on the fracture surface.

■ Failure Mode of AB Joints: In adhesive-bonded joints subjected to tensile-shear forces, two primary failure modes are usually observed: adhesive failure and cohesive failure. Adhesive failure occurs at the interface between the adhesive and one of the adherend materials, while cohesive failure refers to a rupture occurring within the adhesive itself (Refs. 14, 17). The manner in which adhesive-bonded joints fail is influenced by the interplay between the adhesion strength at the adhesive/substrate interface and the inherent strength of the adhesive layer. A detailed analysis of the fracture surface in the Al/Ti adhesive-bonded joint revealed a mixed adhesive/cohesive failure mode, as depicted in Fig. 6B. The proportions of each failure mode were quantified on both fracture surfaces using ImageJ software. Adhesive failure accounted for 36.9  $\pm$  10.3% on the Ti side and 56.6  $\pm$  8.6% on the Al side, while cohesive failure within the adhesive layer constituted 7.4  $\pm$  1.5%.

- Failure Mode of HB Joints: The fracture surface of the dissimilar Al/Ti hybrid-bonded (HB) joint is illustrated in Fig. 6C. Figure 8 presents SEM fractography of the Al/Ti HB joint, with Figs. 8A and B showing the Ti side and Figs. 8C and D showing the Al side. As shown in Fig. 8D, the fracture surface exhibited the presence of pores, voids, and cracks. As depicted in Figs. 8A and C, the fracture surfaces revealed four distinct regions:
- 1. Fracture in the metallurgical bonding zone: characterized by interfacial failure within the brazed region.
- 2. Adhesive-free zone: A region where the adhesive is displaced from the weld area due to the electrode force applied during the squeeze time.
- 3. Heat-affected degradation zone: A zone within the adhesive layer where the adhesive has decomposed or degraded due to excessive heat generated during RSW.
- 4. Adhesive bonding failure zone: exhibiting a mixed adhesive/cohesive failure mode.

## **Discussion**

# Melting Phenomena and Joining Mechanism

The microstructural analysis of the dissimilar Al/Ti RSW and HB joints revealed two distinct melt zones: a central melt zone with columnar grains (Fig. 2A) and martensitic transformation (Fig. 2B) in the middle of the Ti-6Al-4V sheet and a cap-shaped melt region (Fig. 2C) with dendritic structure in the AA6061 aluminum alloy side (Fig. 2D). A continuous, ultra-thin reaction layer approximately 200 nm thick was observed at the Al/Ti interface (Fig. 3C). These observations highlight the complex thermal and metallurgical interactions that occur due to the contrasting physical properties of aluminum and titanium.

- 1. Melting in Ti sheet: The formation of a large melt zone in the Ti-6Al-4V sheet, despite its high melting point, could be attributed to its high electrical resistivity and low thermal conductivity, which led to localized heat accumulation under the applied welding current.
- 2. Melting in Al sheet: The melting of the AA6061 sheet, despite its lower resistivity, resulted from the conductive heat transfer from the hot titanium sheet. It is noteworthy that when welding similar Al/Al materials with a current of 13 kA, no weld nugget forms due to the low electrical resistivity of the aluminum. In contrast, during the Al/Ti RSW process, the AA6061 sheet underwent melting. The Ti-6Al-4V sheet is the primary heat source in dissimilar Al/Ti welding. A thermal gradient across the joint thickness facilitates heat transfer from the Ti-6Al-4V sheet to the aluminum sheet through conduction. This heat transfer is further amplified by the high thermal conductivity of aluminum, which, combined with its lower melting point, causes the aluminum to melt.
- 3. Joining mechanism: As illustrated in Figs. 3A and B, the Ti sheet remained solid at the Ti/Al interface. This phenomenon occurred because the aluminum sheet acted as a heat sink,

preventing the titanium from melting at the interface. As a result, a liquid/solid interface formed between the molten aluminum and the solid titanium. During the joining process, the molten aluminum spread across the solid titanium sheet, suggesting that metallurgical bonding between aluminum and titanium in RSW occurs through a brazing mechanism.

4. Joint interface: The ultra-thin reaction layer observed at the Al/Ti interface was likely an intermetallic compound (IMC) layer that played a critical role in joint formation. Although direct confirmation via TEM is not available, prior studies (Refs. 10, 11, 28-30) on Al/Ti dissimilar joints suggest that IMC formation is plausible. When solid Ti comes into contact with molten Al during joining, Ti atoms begin to dissolve and diffuse into the molten Al. However, the solubility of Ti in liquid Al is extremely low, so the Al rapidly becomes saturated with Ti. Once this saturation limit is exceeded, excess Ti atoms react with Al to form an in-situ solid IMC layer. According to the Al-Ti phase diagram (Ref. 31), TiAl, is the most thermodynamically favorable phase to form under Al-rich conditions. In RSW, the rapid thermal cycle and, consequently, the limited time for solid/liquid reaction, restricts the growth of this layer, resulting in an extremely thin IMC. While this thin layer may aid metallurgical bonding, its intrinsic brittleness can still impair mechanical performance.

5. Defect formation: The voids formed at the joint interface, particularly in the solid-liquid contact zones (see Figs. 4, 7, and 8), suggest insufficient wetting of the solid Ti by the molten Al and a potential localized lack of metallurgical bonding. Such defects are detrimental to mechanical performance, especially under tensile-shear loading. Additionally, the expulsion of molten Al can also lead to the formation of voids at the joint interface. Notably, in the case of HB joints, the presence of residual adhesive at the interface can increase susceptibility to molten metal expulsion and the associated defect formation. Furthermore, short microcracks were observed near these voids (see Figs. 4 and 7). The formation of cracks near voids was likely due to differential thermal contraction during cooling. The mismatch in the coefficient of thermal expansion between Al and Ti generated significant thermal stresses during solidification and cooling, which can initiate and propagate cracks in regions of stress concentration, such as void boundaries. These thermal stresses are further intensified under the rapid solidification conditions characteristic of RSW, particularly where bonding is non-uniform.

## **Key Factors Influencing Mechanical Performance**

The mechanical behavior of Al/Ti joints produced by resistance spot welding, adhesive bonding, and hybrid-bonding is governed by the interplay between bonding mechanisms, interfacial integrity, and failure characteristics. This section integrates the analysis of tensile-shear results, observed failure modes, and the key factors controlling joint performance.

Among the three joining methods, RSW joints exhibited the weakest mechanical performance, characterized by the lowest peak load and limited energy absorption capacity, along with a distinct interfacial failure mode. This inferior behavior was primarily attributed to two key factors: the suspected formation of brittle intermetallic compounds at the joint interface

and the presence of voids. These brittle phases, if present, can severely compromise the toughness of the interface. In combination with interfacial voids, these features disrupt metallurgical bonding and create local stress concentrators that facilitate crack initiation and propagation, ultimately leading to premature failure under mechanical loading.

The HB joints demonstrated significantly superior mechanical performance compared to the RSW joints, exhibiting approximately 2.9-times greater load-bearing capacity and more than 20-times higher energy absorption. This improvement arose from three key mechanisms:

- 1. The adhesive layer provided intrinsic bonding strength and was the primary load-bearing component.
- 2. The adhesive promoted uniform stress distribution across the overlap area, reducing stress concentrations and delaying the onset of failure.
- 3. The RSW process supplemented this by generating localized metallic bonding at the Al/Ti interface through a brazing mechanism.

Fractographic analysis revealed that the HB joints exhibited mixed-mode failure, including adhesive, cohesive, and localized interfacial fracture regions. These complex failure paths indicated multiple crack-arrest mechanisms and progressive damage accumulation, which together contributed to the elevated energy absorption capacity of the joint. This contrasted with the primarily interfacial failure observed in the RSW joints, which suggests brittle fracture with minimal plastic deformation.

The mechanical comparison between the AB and HB joints showed statistically similar peak load values, despite the additional metallurgical bonding introduced by RSW in the HB joints. This similarity can be explained by the competing effects associated with RSW:

- 1. Positive contribution: The solid/liquid reaction at the joint interface enhances the load-bearing capacity by forming a metallurgical bond between the aluminum and titanium sheets.
- 2. Negative contribution: The epoxy adhesive undergoes thermal degradation due to the heat generated during resistance spot welding, which reduces its effectiveness in contributing to the overall load-bearing capacity of the joint. This explains the limited peak load improvement despite the metallurgical bond, as the load-bearing capacity of the adhesive was compromised.

These opposing effects — strengthening via metallurgical bonding and weakening due to adhesive degradation — likely offset each other, leading to the observed parity in peak load between the HB and AB joints.

While the peak load capacities of the AB and HB joints were similar, the energy absorption values revealed a potentially meaningful distinction. The HB joints consistently exhibited higher energy absorption (27.18  $\pm$  5.26 J) than the AB joints  $(17.65 \pm 1.49 \, \text{J})$ , even though the difference did not reach statistical significance (p = 0.13). This lack of significance was likely attributable to the limited sample size and inherent variability in the HB group. However, the large Cohen's d value of 2.3 indicated a large effect size, suggesting a strong practical difference between the two joint types. Therefore, despite the limited statistical confidence, the observed trend

and large effect size highlight the mechanical toughness advantage of HB joints, particularly for applications demanding high energy absorption. Future studies with larger sample sizes and reduced variability are recommended to confirm this trend and establish statistical robustness.

It is worth noting that the metallurgical bond formed in HB joints primarily enhances resistance to normal (tensile) stresses at the Al/Ti interface, whereas the adhesive layer predominantly resists shear loading (Ref. 32). To fully elucidate this combined behavior, future investigations should incorporate cross-tension or coach-peel testing to assess joint response under different stress states.

Several key aspects must be optimized to improve the mechanical performance and reliability of hybrid-bonded Al/Ti joints. The observed high incidence of adhesive failure, particularly on the aluminum side, suggests that the bonding at the adhesive/substrate interface was weaker than the cohesive strength of the adhesive itself. In contrast, the limited cohesive failure indicates that the bulk adhesive possessed adequate intrinsic strength, making interfacial adhesion the primary limiting factor in joint performance. Interfacial adhesion is strongly influenced by surface preparation (Refs. 33-35). This study applied a three-stage surface treatment to both substrates: initial degreasing with acetone to remove organic contaminants, mechanical abrasion via scratch brushing to disrupt and remove the native oxide layer, and a final acetone degreasing step to ensure surface cleanliness. While this approach effectively eliminates surface contamination and increases roughness, promoting mechanical interlocking may not be sufficient to create a chemically stable and adherent oxide layer on the aluminum surface. Due to the tendency of aluminum to rapidly reform a native oxide layer after abrasion, the resulting oxide may be non-uniform or loosely bonded, contributing to interfacial weakness. To overcome this limitation, more advanced surface treatments, such as phosphoric acid anodizing, could be employed to produce a porous, chemically stable oxide layer that enhances adhesive bonding on the aluminum side (Ref. 36). Second, the thermal effects of the resistance spot welding process must be carefully managed. Excessive heat input can lead to expulsion and thermally degrade the adhesive, leading to unbonded zones within the joint. Third, the HB joint exhibited a higher standard deviation in energy absorption, reflecting its greater sensitivity to process control. Tight process control and consistent adhesive application will reduce defect rates and improve reproducibility.

### Conclusions

This work demonstrated that metallurgical bonding between AA6061 aluminum alloy and Ti-6Al-4V titanium alloy can be achieved through resistance spot welding, primarily via a solid-liquid interaction at the interface resembling a brazing mechanism. However, the resulting RSW joints exhibited limited mechanical performance, with low peak load and poor energy absorption. A hybrid-bonding approach — combining RSW with adhesive bonding - significantly enhanced mechanical performance, increasing peak load and energy absorption by 2.9 and 20 times, respectively, compared to conventional RSW joints. Further improvements in hybrid

joint performance may be achieved by enhancing interfacial adhesion through advanced surface preparation techniques and minimizing thermal degradation of the adhesive during welding; for example, by optimizing welding parameters or employing heat-resistant adhesives.

#### References

- 1. Pouranvari, M. 2017. Critical assessment 27: Dissimilar resistance spot welding of aluminium/steel: Challenges and opportunities. *Materials Science and Technology* 33(15): 1705–1712.
- 2. Taghavi, S., and Pouranvari, M. 2023. Spinodal liquid phase separation enabling dissimilar resistance spot welding of immiscible iron and copper alloy system. *Science and Technology of Welding and Joining* 28(2): 98–107.
- 3. Tang, Z., Yang, H., Wan, L., Ren, P., Zhang, X., Wu, Y., Wang, H., and Wang, H. 2024. Blue laser conduction welding of dissimilar Cu and Al sheets. *Welding Journal* 103(7): 203-s to 214-s.
- 4. Zare, M., and Pouranvari, M. 2021. Metallurgical joining of aluminium and copper using resistance spot welding: Microstructure and mechanical properties. *Science and Technology of Welding and Joining* 26(6): 461–469.
- 5. He, H., Gou, W., Lin, S., Yang, C., and Mendez, P. 2019. GTA weld brazing a joint of aluminum to stainless steel. *Welding Journal* 98(12): 365-s to 378-s.
- 6. Lu, Y., Zhang, K., Tran, J., Mayton, E., Kimchi, M., and Zhang, W. 2019. Optimizing ultrasonic plus resistance spot welding for dissimilar metal joining. *Welding Journal* 98(9): 273-s to 282-s.
- 7. Qiu, R., Zhao, P., Zhao, J., Shi, H., and Yu, H. 2023. Resistance element welding of aluminium alloy and steel using an element of aluminium. *Science and Technology of Welding and Joining* 28(8): 766–774.
- 8. ASM Handbook, Volume 2. Properties and selection: Nonferrous alloys and special-purpose materials.
- 9. Zhou, J., Zhou, D., and Liu, J. 2022. Effect of oscillating laser beam on the interface and mechanical properties of Ti/Al fusion welding joint. *Journal of Materials Research and Technology* 19:1993–2007.
- 10. Tian, R., Chen, S., Yang, B., Wu, J., Li, P., Chen, N., Li, H., Wang, Q., Xia, H., and Ma, N. 2023. Elemental diffusion, atomic substitution mechanisms and interfacial fracture behavior in laser welded–brazed Al/Ti. *Materials Characterization* 202: 112998.
- 11. Zhang, Z., Huang, J., Yao, C., and Zhang, X. 2022. Effect of Ag alloying on the microstructure and mechanical properties of laser welded-brazed Ti/Al dissimilar joints. *Materials Science and Engineering: A* 848: 143359.
- 12. Li, Y., Zhang, Y., and Luo, Z. 2015. Microstructure and mechanical properties of Al/Ti joints welded by resistance spot welding. *Science and Technology of Welding and Joining* 20: 385–394.
- 13. Li, Y., Zhang, Y., Bi, J., and Luo, Z. 2015. Impact of electromagnetic stirring upon weld quality of Al/Ti dissimilar materials resistance spot welding. *Materials & Design* 83: 577–586.
- 14. Yacobi, B. G., Martin, S., Davis, K., Hudson, A., and Hubert, M. 2002. Adhesive bonding in microelectronics and photonics. *Journal of Applied Physics* 91: 6227–6262.
- 15. Pouranvari, M., and Safikhani, E. 2018. Mechanical properties of martensitic stainless steel weld/adhesive hybrid bonds. *Science and Technology of Welding and Joining* 23: 227–233.
- 16. Bai, J., Yang, S., Lin, Z., and Yin, Q. 2022. Laser Joining of CFRTS and steel by interfacial pressure control. *Welding Journal* 101(11): 281-s to 288-s.
- 17. Messler, R. W. 2004. *Joining of materials and structures. From Pragmatic Process to Enabling Technology.* Oxford: Butterworth-Heinemann.

- 18. Liu, L.-M., Wang, H.-Y., and Zhang, Z.-D. 2007. The analysis of laser weld bonding of Al alloy to Mg alloy. *Scripta Materialia* 56: 473–476.
- 19. Miyamoto, K., Nakagawa, S., Sugi, C., Ogura, T., and Hirose, A. 2016. Seal spot welding of steel and aluminium alloy by resistance spot welding: Dissimilar metal joining of steel and aluminium alloy by Zn insertion. *Welding International* 30: 675–687.
- 20. Kang, J., Chen, Y., Sigler, D., Carlson, B., and Wilkinson, D. S. 2016. Effect of adhesive on fatigue property of Aural2 to AA5754 dissimilar aluminum alloy resistance spot welds. *Engineering Failure Analysis* 69: 57–65.
- 21. Chen, N., Wang, H. P., Wang, M., Carlson, B. E., and Sigler, D. R. 2019. Schedule and electrode design for resistance spot weld bonding Al to steels. *Journal of Materials Processing Technology* 265:158–172.
- 22. Wang, S., Li, Y., Yang, Y., Manladan, S. M., and Luo, Z. 2021. Resistance element welding of 7075 aluminum alloy to Ti6Al4V titanium alloy. *Journal of Manufacturing Processes* 70: 300–306.
- 23. Niu, S., Wang, Z., Lou, M., Ma, Y., Lei, H., and Li, Y. 2023. Resistance rivet welding of aluminum/titanium dissimilar materials. *Journal of Manufacturing Processes* 108: 141–152.
- 24. AWS D17.2/D17.2M-2019. Specification for resistance welding for aerospace applications. American Welding Society.
- 25. Cohen, J. 1990. Things I have learned (so far). *American Psychologist* 45: 1304–1312.
- 26. Cohen, J. 1988. Statistical power analysis for the behavioral sciences, 2nd ed. Hillsdale, N.J.: Lawrence Erlbaum Associates.
- 27. Pouranvari, M., and Marashi, S. P. H. 2013. Critical review of automotive steels spot welding: process, structure and properties. *Science and Technology of Welding and Joining* 18: 361–403.
- 28. Jiang, S. Y., and Zhang, L. 2013. Microstructure evolution of Al–Ti liquid–solid interface. *Transactions of Nonferrous Metals Society of China* 23: 3545–3552.
- 29. Liu, S., Chew, Y., Weng, F., Sui, S., Du, Z., Man, Y., Ng, F. L., and Bi, G. 2022. Effects of laser pulse modulation on intermetallic compounds formation for welding of Ti-6Al-4V and AA7075 using AA4047 filler. *Materials & Design* 213: 110325.
- 30. Chen, S., Li, L., Chen, Y., and Huang, J. 2011. Joining mechanism of Ti/Al dissimilar alloys during laser welding-brazing process. *Journal of Alloys and Compounds* 509: 891–898.
- 31. Okamoto, H. 2000. *Phase diagrams for binary alloys*. ASM International.
- 32. Li, M., Wang, Y., Tao, W., and Yang, S. 2023. A novel strategy for realizing reliable welding of aluminum-steel. *Welding Journal* 102(12): 293-s to 312-s.
- 33. Comyn, J. 1990. Surface treatment and analysis for adhesive bonding. *International Journal of Adhesion and Adhesives* 10:161–165.
- 34. Leena, K. K. K. A., Athira, K. K., Bhuvaneswari, S., Suraj, S., and Rao, V. L. 2016. Effect of surface pre-treatment on surface characteristics and adhesive bond strength of aluminium alloy. *International Journal of Adhesion and Adhesives* 70: 265–270.
- 35. Rudawska, A., Sikora, J. W., Müller, M., and Valášek, P. 2020. The effect of environmental ageing at lower and sub-zero temperatures on the adhesive joint strength. *International Journal of Adhesion and Adhesives* 97: 102487.
- 36. Sabau, A., Liu, H., Weibel, J. A., Groll, E. A., and Geoghegan, P. 2017. *Surface preparation techniques for adhesive bonding of aluminum and copper* (No. ORNL/TM-2017/196). Oak Ridge National Laboratory, Oak Ridge, Tenn.

**MAHDI HAMRAH** and **MAJID POURANVARI** (pouranvari@ sharif.edu) are with the Department of Materials Science and Engineering, Sharif University of Technology, Tehran, Iran.